Journal of Saudi Chemical Society (2022) **26**, 101446

King Saud University

Journal of Saudi Chemical Society

www.ksu.edu.sa
www.sciencedirect.com

ORIGINAL ARTICLE

The role of 1-octyl-3-methylimidazolium hexafluorophosphate in anticorrosion coating formula development

Zeping Wang [a], **Binjie Hu** [a,*], **George Zheng Chen** [b]

[a] *Department of Chemical & Environmental Engineering, University of Nottingham Ningbo China, 199 Taikang East Road, Ningbo 315000, China*
[b] *Department of Chemical and Environmental Engineering, Advanced Materials Research Group, Faculty of Engineering, University of Nottingham, Nottingham NG7 2RD, United Kingdom*

Received 4 January 2022; revised 11 February 2022; accepted 27 February 2022
Available online 3 March 2022

KEYWORDS

Ionic liquid;
Miniemulsion polymerization;
Polymer;
Anticorrosion;
Coating;
Formulation

Abstract A hydrophobic ionic liquid (1-octyl-3-methylimidazolium hexafluorophosphate, C_8mimPF_6) with a function of inhibiting corrosion was encapsulated at different concentrations in the copolymer of poly (methyl methacrylate) and poly (butyl acrylate) through miniemulsion polymerization. These latexes were coated on steel samples whose corrosion properties were evaluated by electrochemical techniques. It was found that increasing the C_8mimPF_6 concentration from 0 wt% to 30 wt%, the corrosion inhibition efficiency was remarkably improved from 41% to 89% based on the charge transfer resistance and from 64% to 87% based on the corrosion current density, respectively. The ionic liquid did not attend the reaction during latex preparation but behaved as corrosion inhibitors on the steel surface. Such an anticorrosion effect could be ascribed to the physical adsorption of the C_8mim^+ cation on the reaction sites and the hydrophobicity enhancement resulting from the hydrophobic PF_6^- anion.

1. Introduction

Nowadays, considerable research on waterborne coatings has been policy-driven to find alternative routines to the minimization of emission of volatile organic compounds (VOCs) [1–6]. Acrylic coatings are widely used due to their low cost and unique properties, such as excellent adhesion, coalescence, color retention and resistance to hydrolysis and chemical inertness under ultraviolet radiation [7,8]. However, different from solvent-based coatings, waterborne acrylic coatings are still unsatisfactory, especially the anticorrosion performance in a salty environment. This is largely due to the hydrophilic groups in the formed coatings being affinitive to water, oxygen and chloride ions and easily inducing corrosion [9]. To overcome this problem, addition of inhibitors to enhance corrosion resistance can be an easy choice.

* Corresponding author.
E-mail address: Binjie.HU@nottingham.edu.cn (B. Hu).
Peer review under responsibility of King Saud University.

Production and hosting by Elsevier

https://doi.org/10.1016/j.jscs.2022.101446

Traditional corrosion inhibitors are toxic such as chromates [10,11]. More alternatives were later developed such as plant extracts and drugs which still require large amount of volatile organic solvents during the extraction process [12]. In contrast, ionic liquids (ILs) with specific properties such as extremely low vapor pressure, high thermal stability and flame resistance, high conductivity and wide electrochemical window could be better alternative corrosion inhibitors [13]. ILs are often composed of large asymmetric organic cations and inorganic or organic anions. Some specific requirements such as hydrophobicity can be achieved by adjusting the anions [14]. There were some research about the applications of ILs in corrosion inhibition, mainly hydrophilic one. Ashassi-Sorkhabi and Es'haghi [15] reported that a simple IL, 1-butyl-3-methylimidazolium bromide ([BMIM]Br), could inhibit the corrosion of mild steel in 1 M hydrochloric acid, which was evaluated by weight loss and electrochemical techniques. As a corrosion inhibitor, [BMIM]Br could spontaneously adsorb on the surface of mild steel with electrostatic force between $BMIM^+$ and negatively charged mild steel surface, which suppressed the corrosion reaction at both the catholic and anodic sites, offering improved corrosion resistance at higher IL concentrations. Moreover, the inhibition performance of ILs is influenced by the cation, anion and structure of ILs (e.g. chain length). Al-Rashed and Nazeer [16] compared the inhibition efficiency of ILs in 1 M hydrochloric acid with different cations (i.e. imidazolium, pyridinium, and pyrrolidinium) and the same anion, and stated that imidazolium was the optimal cation with highest inhibition efficiency due to the larger molecular size and delocalization of aromatic moieties. Subsequently, they also studied the effect of alky chain length on inhibition properties and concluded that longest alkyl chain contributed to the highest protection efficiency. One explanation of this is that the surface coverage of ILs was increased due to the enhanced adsorption when applying ILs with longer alkyl chains [17]. It is known that heteroatoms (such as O, N, S and P), heterocyclic rings or conjugated unsaturated bonds in organic inhibitors play an essential role in corrosion inhibition performance [18]. For example, in a corrosive environment, ILs can adsorb onto the surface of mild steel by either physical adsorption or chemical adsorption, sometimes even both. The reaction sites on the substrate are blocked by adsorbed ILs so that the mass and charge transfer are hindered and corrosion inhibition is achieved [19,20]. For imidazolium ILs, there are two proposed reaction routines towards anticorrosion. According to Likhanova, et al. [21], In routine 1, cation of ILs can inhibit both anodic and cathodic sites by forming a complex on the substrate surface. Anions of corrosive medium would adsorb on anodic sites due to the limited amount of anion of ILs compared with corrosive ions. Subsequently, adsorbed species interacted with cation of ILs and formed a complex covered on the substrate. At the same time, on the cathodic sites, cation of ILs could replace the cations of corrosive medium and occupy the reaction sites because of the larger steric hindrance itself. There was a free pair of electrons left in N atom of imidazolium group, which could be donated to the metal surface. In routine 2, the initial stage was similar as routine 1 that anions of corrosive medium adsorbed on cathodic sites of metal surface and the surface became negatively charged. Then the cation of ILs would be physically adsorbed via electrostatic force. Meanwhile, the anion of ILs could subsequently adsorb on the anodic sites via chemical adsorption [22–24]. The main difference between these two proposed routines is the adsorption type of cations of ILs on cathodic sites and attendance of anions of ILs.

The aforementioned research has proven the inhibition effect of ILs. However, all the research mentioned above directly dissolved the hydrophilic ILs in the bulk solution, relying on the ILs to spontaneously adsorb on the surface of substrate for protection. Since our research is for marine anticorrosion application, dissolving a large quantity of ILs into the sea is not realistic, which would not only increase the overall cost for the product but also cause harmful impact to the surrounding open marine environment. A more efficient formula is desired to confine the functioning ILs on the surface of the metal to be protected, such as incorporation of ILs into a polymer coating [25]. Using a hydrophobic IL to replace the traditional hydrophilic IL could be a solution to overcome hydrophilicity of ILs.

C_8mimPF_6 is a conventional hydrophobic IL with solubility (mole fraction) 1×10^{-4} in water [26]. PF_6^- is a typical hydrophobic anion and C_8mim^+ is a one kind of imidazolium cations with relatively long alky chain. As mentioned above, inhibition performance of imidazolium cations is better than other cations and the longer alky chain in imidazolium leads to prior inhibition effect [16]. Therefore, C_8mimPF_6 was chosen as the corrosion inhibitor for this research. To effectively introduce C_8mimPF_6 into waterborne coating formula without losing its corrosion function, this research was designed to encapsulate the hydrophobic IL, 1-octyl-3-methylimidazolium hexafluorophosphate (C_8mimpF_6), into copolymer of poly(methyl methacrylate) (PMMA) and poly (butyl acrylate) (PBA) synthesized via miniemulsion polymerization in which the monomers were directly polymerized in the oil droplets, rather than being transferred from droplets to micelles as described in the conventional emulsion polymerization [27]. Furthermore, the latex from miniemulsion polymerization was more stable than those developed through conventional emulsion polymerization [3]. To the best of our knowledge, we are the first authors to encapsulate hydrophobic ILs into copolymer via miniemulsion polymerization for anticorrosion application in 3.5 wt% NaCl solution. The roles of C_8mimPF_6 in the PMMA/PBA copolymer were revealed by further polymer characterizations.

2. Experimental

2.1. Materials

Methyl methacrylate (MMA, CP), L-Ascorbic acid (AAc, AR), hydrogen peroxide (H_2O_2, AR), and sodium dodecyl sulfonate (SDSO, CP) were supplied by Sinopharm Chemical Reagent Co Ltd. Hexadecane (HD, 98%), and n-butyl acrylate (BA, 99%) were purchased from Aladdin Industrial Inc. 1-octyl-3 methylimidazolium hexafluorophosphate (C_8mimPF_6, 95%) was from Shanghai Cheng Jie Chemical Co Ltd. Ultra-pure water with a resistivity of 18.2 MΩ·cm was made in house. The testing metal sample, i.e., mild steel Q235 was bought from Shenzhen Zhi Bao Metal Products Co., Ltd. The mild steel composition (wt%) is 0.14–0.22 C, 0.3–0.65 Mn, <0.30 Si, <0.04 5P, <0.055 S, and Fe rest.

2.2. Preparation of miniemulsion

This was carried out by preparing the oil (5 wt% HD and 95 wt% MMA/BA/C_8mimPF_6) and water (30 mM SDSO) phases before mixing. The oil phase was prepared by first mixing MMA and BA with a fixed ratio of 1:1, followed by adding C_8mimPF_6 with various desired concentrations into the oil phase. The oil phase was then added into the water phase with an O/W volume ratio of 3:7, and then transferred in a sonicator (Xinzhi Scientz II) for homogenization. The ultrasonication time was set as 6 min at a power input of 285 W in a manner of 1 s on and 1 s off.

2.3. Miniemulsion polymerization

The newly formed miniemulsion described in session 2.2 was transferred into a 250 mL four-necked flask equipped with a stirrer, a reflux condenser, a thermometer, and sparged with nitrogen for miniemulsion polymerization with the reaction temperature being controlled by a water bath. Nitrogen was bubbled through for 1.5 h at the beginning of the reaction to remove oxygen until the reactant temperature reached the desired value. The agitation speed of the stirrer was set at 200 rpm throughout the reaction process. The H_2O_2/AAc solution in the molar ratio of 1.0 to 1.3 was injected to start the reaction.

2.4. Characterization

2.4.1. FTIR

FTIR spectra of dried latex samples were collected from the Bruker vertex 70 instrument.

2.4.2. Electrochemical techniques

Mild steel specimens with 1 cm in length and 1 cm in width were selected as the substrate for coating. After the treatment with the emery paper, several drops of latex developed from previous steps were dropped on the one side of surface of mild steel specimen followed by the rolling of bar coater BGD212/150 μm from the side to the other side evenly. After evaporation of water, the solid content remained, the film thickness was measured with a PosiTectorFS1 apparatus, and the thickness was approximately 40 ± 2 μm.

The anticorrosion performance of coatings was evaluated with CHI-660E electrochemical workstation. A three-electrode cell of 30 mL in volume was made in-house and used. In the cell, the coated mild steel electrode was the working electrode with a platinum sheet counter electrode and an Ag/AgCl (in 3.0 M KCl) reference electrode. The electrolyte of the cell was an aqueous solution of 3.5 wt% NaCl. The tests lasted up to 96 h, and electrochemical parameters were recorded every 24 h. For each sample, the open circuit potential (OCP) was measured for 0.5 h before analyses by electrochemical impedance spectroscopy (EIS) and potentiodynamic polarization. EIS was performed at the OCP and frequencies from 10 kHz to 10 mHz under a ±10 mV amplitude sinusoidal voltage. Tafel plots were scanned at a rate of 0.5 mV/s in the range of ±250 mV vs. OCP.

2.4.3. Wettability

The wettability of latex coating was evaluated by measuring the contact angle between water and the latex coated mild steel surface. using the dynamic contact angle measuring instrument. (DCAT21 DataPhysics Instruments Co Ltd).

2.4.4. Surface morphology

Under a 4 kV accelerating voltage, the morphology of coating films was studied by scanning electron microscopy (SEM) (ΣIGMA/VP, Carl Zeiss Microscopy Ltd).

3. Results and discussion

3.1. Anticorrosion performance of PMMA-co-PBA coatings

The latex was prepared as described in Session 2.3 and then coated on the clean mild steel surface as described in Session 2.4. The anti-corrosion performance of coatings containing C_8mimPF_6 were evaluated using various electrochemical techniques like open circuit potential (OCP), electrochemical impedance spectroscopy (EIS) and Tafel polarization curves. The corrosion results were presented via analyzing the impedance and inhibition efficiency. Subsequently, the surface morphology of each sample was inspected after the immersion-corrosion test.

3.1.1. Open circuit potential

The open circuit potential (OCP) can serve as an indicator of cathodic protection of the coating to reveal the extent of electrochemical oxidation when a substance was exposed to a corrosive environment [28]. For a coated mild steel sample immersed in 3.5 wt% NaCl solution, the OCP value may shift negatively when the sample experiences further oxidation. In other words, less positive OCP values means more severe corrosion. In this experiment, the OCP measurement lasted for 30 min until a stable value was reached. The OCP of different coated samples in variation of immersion time were recorded and plotted in Fig. 1. The initial OCP of the bare mild steel, 0 wt% C_8mimPF_6, 1 wt% C_8mimPF_6 and 30 wt% C_8mimPF_6 samples were −523 mV, −496 mV, −492 mV and −357 mV, respectively. This trend of OCP variation indicates that the 30 wt% C_8mimPF_6 sample was under least severe corrosion compared with the others. Among the samples, all coated samples with C_8mimPF_6 from 0 wt% to 30 wt% exhibited more positive OCP than the bare one, which means that all coated sample exhibited higher anticorrosion resistance than the bare one. The OCP values for all samples shifted negatively after 24 h due to the corrosive environment, and then became stabilized. The change of OCP for all samples within 96 h immersion was similar. This means that the initial coating effect dominated the overall anticorrosion effect. A smaller negative shift on OCP of coated samples with higher concentration of C_8mimPF_6 may be attributed to less and slower diffusion of the corrosive species from the bulk solution to the substrate, which indicates that the corrosion inhibition performance was improved with increasing the C_8mimPF_6 concentration [9]. Herein OCP tests were only applied for rough observation of oxidation extent. To quantitatively evaluate the anticorrosion performance, further electrochemical tests were carried out.

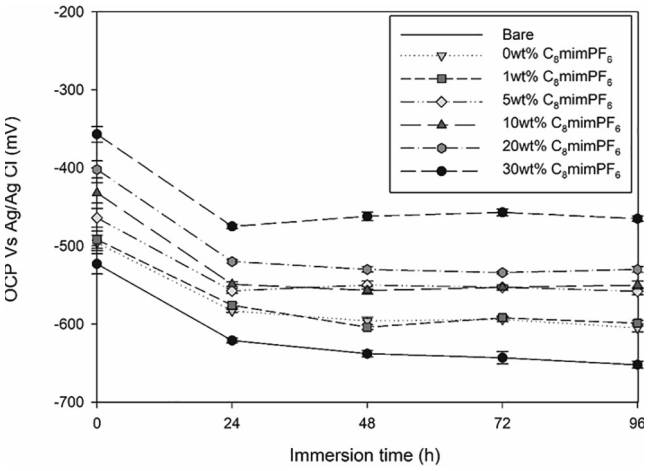

Fig. 1 OCP - time curves for coated electrodes with various concentration of C_8mimPF_6 immersed in 3.5 wt% NaCl solution up to 96 h.

3.1.2. Inhibition performance evaluation based on electrochemical impedance spectroscopy

Electrochemical impedance spectroscopy (EIS) is one of the commonly used methods to evaluate anticorrosion performance. The technique is non-destructive to the coated sample when the measurement is at OCP with low amplitude and in a short period. Differing from the OCP measurement that only gives rough evaluation, the results of EIS could reveal more quantified parameters such as inhibition efficiency and coating electrolyte uptake via the Nyquist plot, where inhibition efficiency represents the anticorrosion performance and coating electrolyte uptake manifests the extent of electrolyte retained in the coating. During the experiment, the degradation of various samples was evaluated by immersing them into the 3.5 wt % NaCl solution for different periods and exhibited as a Nyquist plot after test. Fig. 2 shows the Nyquist plots for mild steel coated with PMMA-co-PBA containing C_8mimPF_6 from 0 wt% to 30 wt%. It appears that there are two semicircles on each plot, indicating two time constants. One is in the high frequency range correlated to the defects and pinholes in the coating, which is shown on the top right side of small figure. The other is in the low frequency range corresponding to charge transfer polarization resistance of the mild steel surface beneath the coating layer [29,30]. The impedance data are modelled against an equivalent circuit shown in Fig. 3. In this figure, the circuit represents the electrode/electrolyte and coating/metal interfaces, where the electrode coating layer is porous [31,32]. Solution resistance (R_s), coating resistance (R_c), coating capacitance (C_c), constant phase element (CPE_{dl}) reflecting the no-ideal capacitance of double layer and charge transfer resistance (R_{ct}) are five essential parameters of this circuit. After nonlinear curve fitting of the data shown in Fig. 2, the parameters at different immersion times excluding the solution resistance were obtained as plotted in Fig. 4.

Impedance could directly imply the anticorrosion performance. Higher coating resistance and charge transfer resistance indicate prior corrosion hindrance [33]. As shown in Fig. 4, in the salty environment, the R_c value of the 30 wt% C_8mimPF_6 sample was 4563 $\Omega{\cdot}cm^2$ at initial stage, which was one order of magnitude higher than the value of other samples with lower concentrations of C_8mimPF_6. Even though the R_c values decreased with the penetration of corrosive ions during immersion, the value at 30 wt% C_8mimPF_6 was still higher than those obtained with other C_8mimPF_6 concentration samples. This suggested that the 30 wt% C_8mimPF_6 sample offered the best corrosion protection performance. Similar results were obtained from the plots of charge transfer resistance, R_{ct} at different immersion times. The R_{ct} value of the 30 wt% C_8mimPF_6 sample at initial stage was 46.3 $k\Omega{\cdot}cm^2$ and always the highest compared with the other samples. Although it decreased with prolonging the immersion time, the final R_{ct} of 0 wt% and 30 wt% C_8mimPF_6 samples were 1.4 $k\Omega{\cdot}cm^2$ and 8.2 $k\Omega{\cdot}cm^2$, respectively. It could be deduced from the final results that R_{ct} of 30 wt% C_8mimPF_6 sample was almost 7 times higher than the value of 0 wt% C_8mimPF_6 sample. Lewis et al. [34] studied the corrosion resistance of a waterborne acrylic coating modified with nano-sized titanium dioxide and stated that the corrosion resistance of acrylic coating with or without modification after the immersion test were approximately 8.0 $k\Omega{\cdot}cm^2$ and 1.0 $k\Omega{\cdot}cm^2$, respectively. Compared with this, the C_8mimPF_6 added in the coating in this work could achieve a similar effect on anticorrosion. Ding et al. [9] used modified lignin dispersed graphene in waterborne epoxy for anticorrosion and the final R_{ct} with or without graphene were 170.0 $k\Omega{\cdot}cm^2$ and 17.8 $k\Omega{\cdot}cm^2$, respectively. This suggests that the waterborne epoxy coating doped with graphene offered much better anticorrosion performance than C_8mimPF_6 encapsulated PMMA-co-PBA latex. The weaker performance of our samples might be caused by the low cross-linking extent of the PMMA-co-PBA coating [35]. Further improvement is possible if more suitable waterborne acrylic coating and ILs were selected. At least, this research opens up a new direction for ILs in waterborne acrylic coating for anticorrosion.

The R_{ct} value could also be used to calculate corrosion inhibition efficiency IE_R as follows [36]:.

$$IE_R\% = \frac{R_{ct}(coated) - R_{ct}(uncoated)}{R_{ct}(coated)} \times 100\% \quad (1)$$

where R_{ct} (coated) and R_{ct} (uncoated) are the charge transfer resistance of the coated and uncoated samples after 96 h immersion. According to the results shown in Table 1, the inhibition efficiency improves from 41% to 89% with increasing the C_8mimPF_6 concentration from 0 wt% to 30 wt%. The improvement is significant, while it may be not as satisfactory as similar anticorrosion coatings in other literature. For instance, Dagdag, et al. [37] studied a polymer based epoxy anticorrosion coating cured with methylene dianiline (TGEDA-MDA) in 3 wt% NaCl solution and stated that the protection efficiency reached 93%. Compared with TGEDA-MDA, the anticorrosion performance of C_8mimPF_6 encapsulated in PMMA-co-PBA was relatively weaker. Possibly the thickness of TGEDA-MDA coating was 170 μm, which was much thicker than the 40 μm PMMA-co-PBA coating.

In addition to the impedance, the aforementioned trend of C_c and CPE_{dl} can be indicative of the permeation of corrosive ions and oxygen to mild steel surface through the pores of the coating layer, which is also called as electrolyte uptake [38]. In this experiment, the main composition of the electrolyte was water. Thus, electrolyte uptake, in other words, can be represented as water absorption. Due to the residue of surfactants in the coating, this PMMA-co-PBA composite tends to absorb

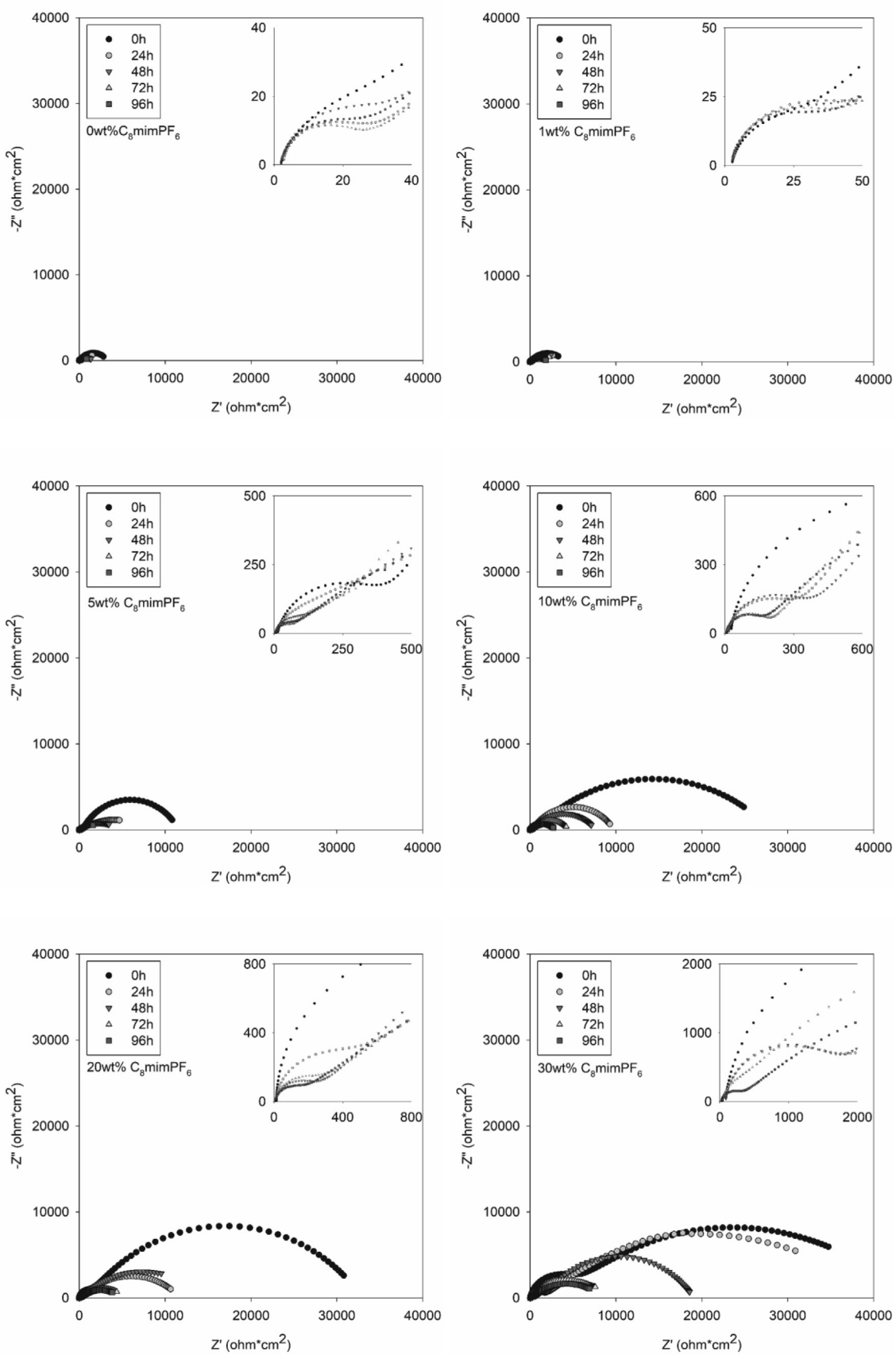

Fig. 2 Nyquist plots of coated electrodes immersed in 3.5 wt% NaCl solution for up to 96 h.

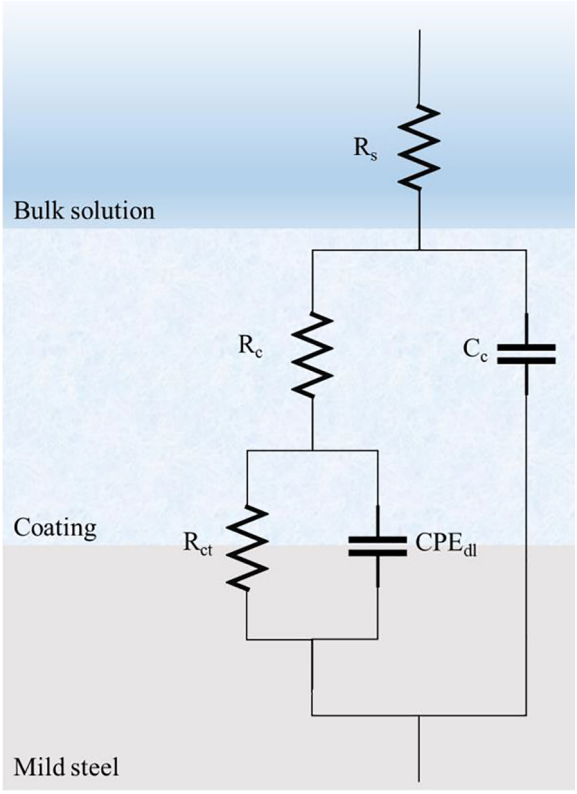

Fig. 3 Equivalent circuit for EIS data fitting.

water. In the immersion test, water dissolved corrosive ions were absorbed into the coating, which changed the charge distribution on the coating surface. Moreover, the introduction of water changed the dielectric constant of the original coating. For instance, the dielectric constants of polymers are usually about 3–8 [39], while the value for water equals to 78.3 at 25 °C [40]. According to the definition equation of capacitance of a capacitor, the capacitance is positively related to the dielectric constant. Therefore, higher electrolyte-uptake ratio is represented as higher coating capacitance and double layer capacitance in equivalent circuit [41]. In summary, the increment of coating capacitance normally results from the charge redistribution or dielectric phenomena in the coating [29]. As shown in Fig. 4b and d, the C_c and C_{dl} values exhibited an increasing trend for all samples based on immersion time with and without C_8mimPF_6, which suggested an increase of corrosive ions passing through the coating.

The electrolyte uptake can be further quantified using the volume fraction of absorbed electrolyte ϕ based on the Brasher and Kingsbury equation [42],

$$\phi\% = \frac{log(\frac{C_t}{C_0})}{log\varepsilon_w} \times 100\% \quad (2)$$

where C_0 and C_t are the coating capacitance at initial stage and time t, respectively. ε_w is the dielectric constant of electrolyte. In this work, water was chosen to prepare the electrolyte, of which, ε_w should be close to 78.3 at 25 °C [40]. The calculated volume fraction of water uptake for each sample at different immersion times is shown in Table 2. Up to 72 h immersion, the 30 wt% C_8mimPF_6 sample exhibited the lowest volume fraction of electrolyte uptake compared with other samples, which manifested the optimal anticorrosion performance at this concentration. However, the water uptake of the 30 wt % C_8mimPF_6 sample sharply increased as immersion time increased from 72 h to 96 h and the value was even higher than that of 20 wt% C_8mimPF_6 samples. This is a sign of coating degradation, which would be further discussed in the mechanism section. Therefore, 30 wt% sample might not be suitable for long term exposure in a salty environment.

In summary, the outcome of EIS is consistent with the results of OCP. Meanwhile, the EIS evaluation of anticorrosion performance mentioned above is based on the comparison of charge transfer or diffusion response of the Nyquist plot. To have better understanding on corrosion inhibition mechanism with different evaluation parameters, for instance, corrosion inhibition efficiency based on corrosion current density, supplementary method like Tafel polarization is required.

3.1.3. Inhibition efficiency evaluation based on the Tafel plot

Tafel plots are unique polarization curves that can provide corrosion-related information between the corrosion current density and corrosion potential. The polarization curves of bare mild steel and coated electrodes immersed in the 3.5 wt % NaCl solution for up to 96 h at room temperature are shown in Fig. 5. It was found that the peaks of all polarization curves shifted to more positive potentials with the increase of C_8mimPF_6 concentration, which is a strong evidence for enhanced anticorrosion effect of the added C_8mimPF_6. In Tafel plots, current density and electrode potential are two essential parameters. After data fitting, the corrosion current density (i_{corr}) and corrosion potential (E_{corr}) were obtained from Tafel extrapolation and listed in Table 3. In this table, anodic and cathodic Tafel slopes b_a and b_c are also listed.

Corrosion inhibition efficiency based on corrosion current density, IE_i, is calculated according to Eq. (3) below,

$$IE_i\% = \frac{i_0 - i}{i_0} \times 100\% \quad (3)$$

where i_0 and i are the corrosion current densities of the bare mild steel and coated electrodes, respectively. Table 3 elucidates a trend of greater corrosion inhibition efficiencies at higher C_8mimPF_6 concentrations. The highest IE_i value in Table 3 is 87% at 30 wt% C_8mimPF_6. However, the IE_i value ceases to increase when the C_8mimPF_6 concentration is above 20 wt% at 86% inhibition efficiency. The inhibition efficiency of the 30 wt% sample was supposed to be higher. One possible explanation is that the less content of PMMA-co-PBA when the concentration of C_8mimPF_6 increased in the oil phase. The further enhancement of C_8mimPF_6 on corrosion was traded off by the content reduction of PMMA-co-PBA, which was the main protection material in the coating.

In addition to inhibition efficiency, corrosion rate (V_{corr}, mm per year) can be also calculated from the corrosion current density via Eq. (4) [43],

$$V_{corr} = \frac{i_{corr}M}{DV} \times 3270 \quad (4)$$

where i_{corr} is the corrosion current density (A/cm^2), M is the atomic or average atomic weight of the metal subjected to corrosion (g·mol^{-1}, M = 56 for mild steel), V is the valence (V = 2 for the oxidation of steel), 3270 (mm·g·A^{-1}·cm^{-1}·year^{-1}) is a constant for unit conversion [44], and D is the density of the corroding metal (g·cm^{-3}, D = 7.85 for mild steel).

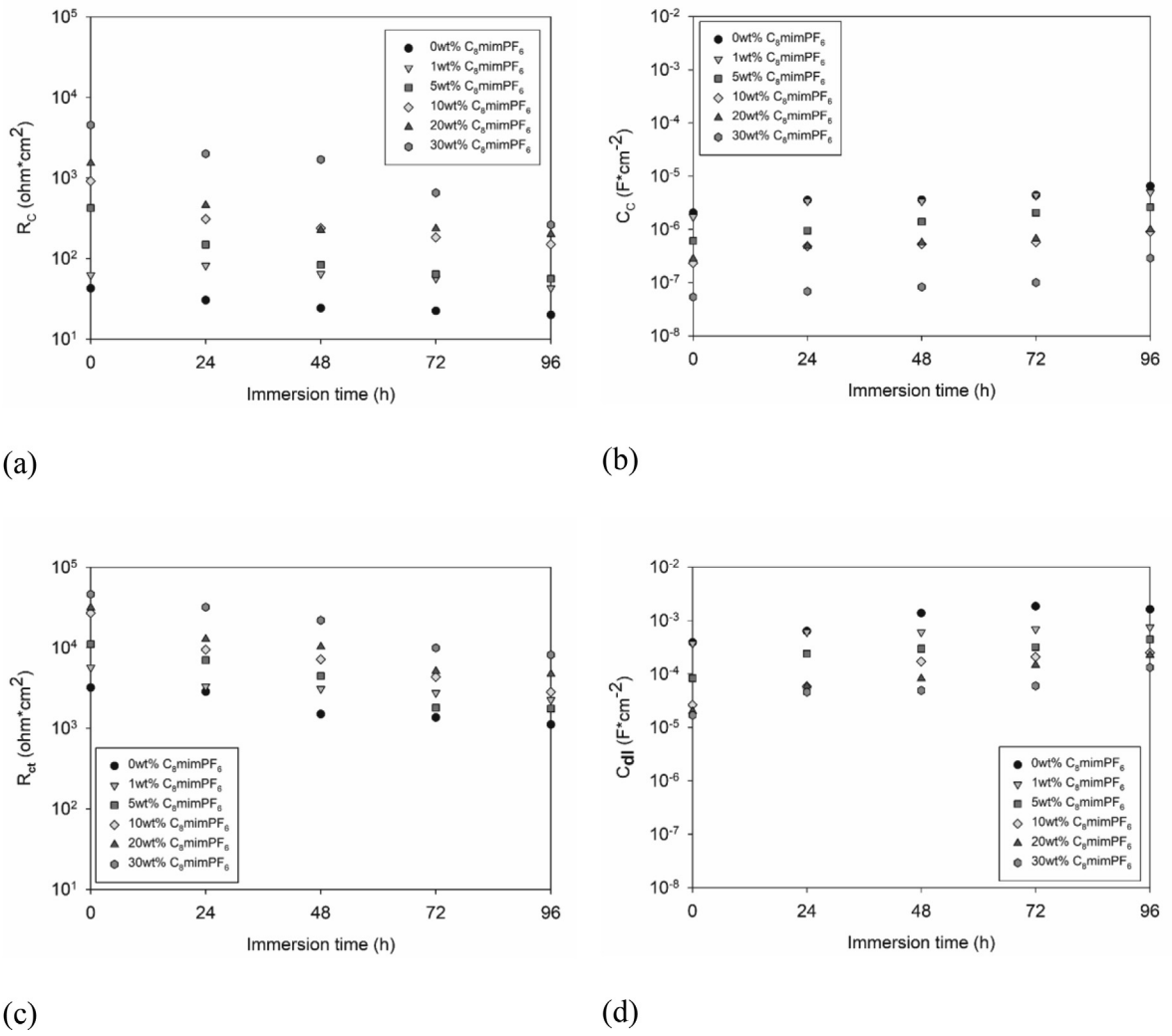

Fig. 4 The evolution of coating resistance (a), coating capacitance (b), charge transfer resistance (c) and double layer capacitance (d) of different coatings immersed in 3.5 wt% NaCl solution up to 96 h.

Table 1 Charge transfer resistance and inhibition efficiency of each samples containing different concentration of C_8mimPF_6 after 96 h immersion test.

Sample	Charge transfer resistance ($\Omega \cdot cm^2$)	Inhibition efficiency
Bare	880	
0 wt% C_8mimPF_6	1489	41%
1 wt% C_8mimPF_6	1752	50%
5 wt% C_8mimPF_6	2065	57%
10 wt% C_8mimPF_6	3042	71%
20 wt% C_8mimPF_6	4912	82%
30 wt% C_8mimPF_6	8171	89%

The corrosion rate V_{corr} is proportional to the corrosion current density. Higher V_{corr} value means worse corrosion inhibition performance. The calculated V_{corr} for samples with various concentrations of C_8mimPF_6 are shown in Table 3. It can be found that the corrosion rate decreased from 1.5×10^{-1} mm per year for the bare sample to 5.5×10^{-2} mm per year at 0 wt% C_8mimPF_6, which was 64% reduction. Then the value decreased by 86% to 2.1×10^{-2} mm per year at 30 wt% C_8mimPF_6, despite that the V_{corr} value already decreased to 2.2×10^{-2} mm per year when the C_8mimPF_6 concentration was 20 wt% and almost no further improvement by further increasing C_8mimPF_6 concentration from 20 wt% to 30 wt%. This is consistent with the conclusion of inhibition efficiency form Tafel plots. Further in-depth discussion on mechanism of C_8mimPF_6 on the corrosion rate will be given in Session 3.2.

3.1.4. Surface morphology of coating layer

After the immersion test as described in 2.4.2, the morphology of each coated mild steel specimen was observed using SEM as shown in Fig. 6. The surface of bare mild steel was observed with the severest corrosion where the rusted area almost covered the whole surface of the mild steel sample. For the steel sample with the coating without C_8mimPF_6, the number of rusts clearly decreased. The notable cracks and pinholes on the surface could be attributed to the defects and micropores formed during the film formation of PMMA-co-PBA that

Table 2 Water uptake of each samples containing different concentration of C_8mimPF_6 immersed up to 96 h.

	Electrolyte uptake (%)				
Samples\time	0 h	24 h	48 h	72 h	96 h
0 wt% C_8mimPF_6	0.0	15.0	17.5	22.8	26.4
1 wt% C_8mimPF_6	0.0	15.7	17.4	21.2	24.4
5 wt% C_8mimPF_6	0.0	15.6	17.5	21.5	23.2
10 wt% C_8mimPF_6	0.0	14.2	16.7	18.9	20.8
20 wt% C_8mimPF_6	0.0	12.8	14.1	16.2	19.9
30 wt% C_8mimPF_6	0.0	5.7	10.0	12.6	21.6

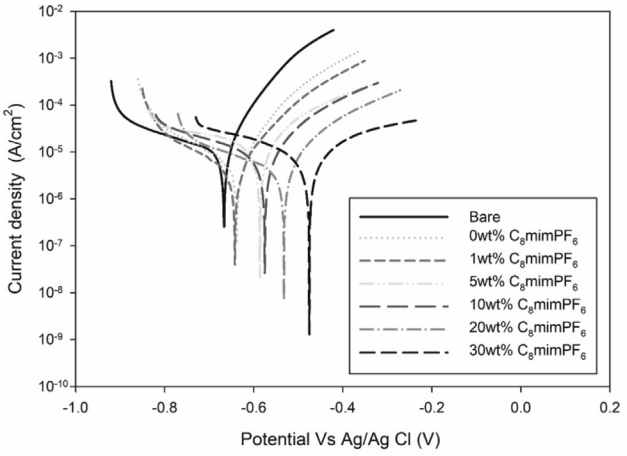

Fig. 5 Tafel polarization plot for bare mild steel and coated electrode immersed in 3.5 wt% NaCl solution up to 96 h.

could be easily penetrated by corrosive ions in the immersion test. Introducing a small amount of C_8mimPF_6, e.g., 1 wt% C_8mimPF_6, cracks were replaced by pits, while severe corrosions were still observed. When the concentration of C_8mimPF_6 rose to 5 wt%, pit corrosion diminished, while flakes that accumulated on the surface still manifested the degradation of coating film. In contrast, it could be seen that the number of defects reduced significantly with increasing the C_8mimPF_6 concentration to 10 wt%. However, there were a few pinholes remaining on the surface. The improvement on anticorrosion in the presence of higher concentrations of C_8mimPF_6 might be ascribed to the barrier effect of C_8mimPF_6 towards the coating film, while there is another possibility that C_8mimPF_6 could behave like a plasticizer forming a film with less defects [45]. The surface morphologies of samples with 20 wt% and 30 wt% C_8mimPF_6 are similar in Fig. 6. This is consistent with the results of R_t evaluation that no difference on corrosion effect between the 20 wt% and 30 wt% C_8mimPF_6 samples, though the latter showed a relatively more smooth film.

3.2. Mechanism of C_8mimPF_6 as corrosion inhibitors

3.2.1. Characterization of C_8mimPF_6 in PMMA-co-PBA

Latex samples containing different concentrations of C_8mimPF_6 were synthesized via miniemulsion polymerization as described in 2.2 and 2.3. The status of C_8mimPF_6 in the polymer was investigated using FTIR spectroscopy. Results are shown in Fig. 7. It has been found that for pure C_8mimPF_6, several characteristic peaks of C_8mim^+ were found. For instance, the peak at 3173 cm^{-1} represents the n(C–H) stretching vibration of the aromatic ring, 1574 cm^{-1} indicates the imidazolium H–C–C bending, 1469 cm^{-1} manifests the imidazolium H–C–N bending and 1168 cm^{-1} refers to the imidazolium C2–N1–C5 bending. For PF_6^-, the peaks at 837 and 558 cm^{-1} represent the P-F stretching and bending vibrations, respectively. As for peaks at 2958, 2930 and 2859 cm^{-1}, they can be assigned to the asymmetric C–H stretching vibration of the CH_3 group, C–H stretching vibration of the alkyl group and symmetric C–H stretching vibration of the CH_2 group [46–48]. Moreover, for the FTIR spectrum of pure PMMA-co-PBA, it could be found that the characteristic band at 2997 cm^{-1} representing the C–H bond stretching vibrations of the $–CH_3$ and 2952 cm^{-1} representing the same stretching for $–CH_2–$ groups. In addition, the peak at 1444 cm^{-1} indicates the bending vibration of the C–H bonds [49]. Peaks at 1732, 1250 and 1150 cm^{-1} can be ascribed to the C–O–C stretching vibration and the presence of carboxyl group in PMMA and PBA [49,50].

Characteristic peaks of C_8mimPF_6 at 3173, 1574, 1168, 837 cm^{-1} and 558 cm^{-1} appeared in all samples containing C_8-

Table 3 Tafel parameters of bare mild steel and coated electrodes immersed in the 3.5 wt% NaCl solution for up to 96 h.

	E_{corr} (mV)	i_{corr} (μA·cm^{-2})	ba (mV·dec^{-1})	bc (mV·dec^{-1})	Inhibition efficiency	V_{corr} (mm per year)
Bare	−667	13.2	127	−335		0.154
0 wt% C_8mimPF_6	−638	4.7	80	−176	64%	0.055
1 wt% C_8mimPF_6	−642	4.2	81	−213	68%	0.049
5 wt% C_8mimPF_6	−586	3.5	56	−108	73%	0.041
10 wt% C_8mimPF_6	−575	3.0	48	−103	78%	0.035
20 wt% C_8mimPF_6	−532	1.9	47	−118	86%	0.022
30 wt% C_8mimPF_6	−474	1.8	52	−63	87%	0.021

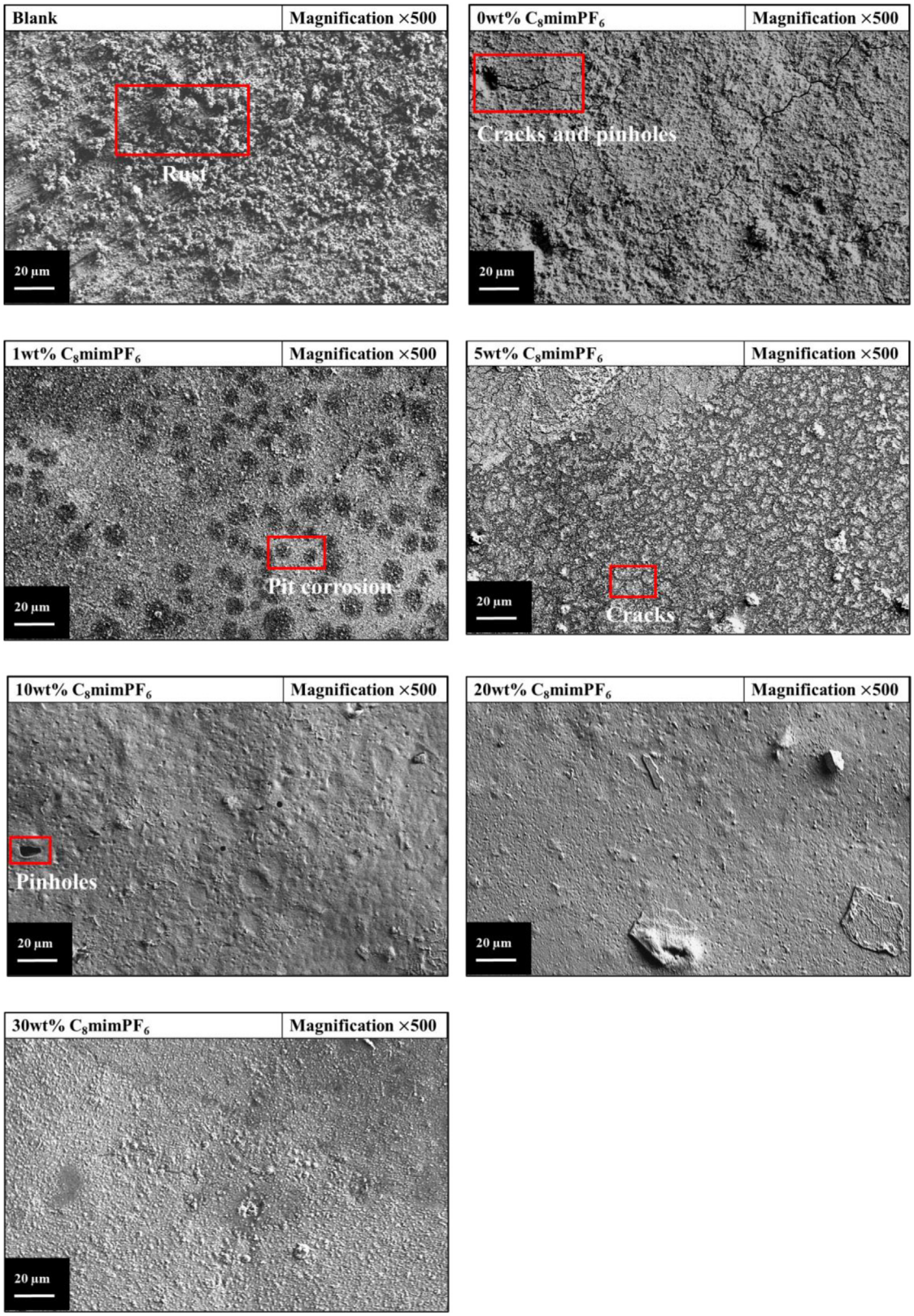

Fig. 6 SEM image angle as a function of IL (C_8mimPF_6) concentration after 96 h immersion in 3.5 wt% NaCl solution.

$mimPF_6$ e.g., 10, 20 and 30 wt%, which confirms the existence of C_8mimPF_6 in the PMMA-co-PBA matrix. However, no new peaks were observed in comparison with those spectra of pure PMMA-co-PBA and pure C_8mimPF_6. This is not surprising. For free radical polymerization, the double bonds like carbon–carbon double bond in vinyl monomers and the carbon–oxygen double bond in aldehydes and ketones are essential to radical initiators [51]. However, for C_8mimPF_6,

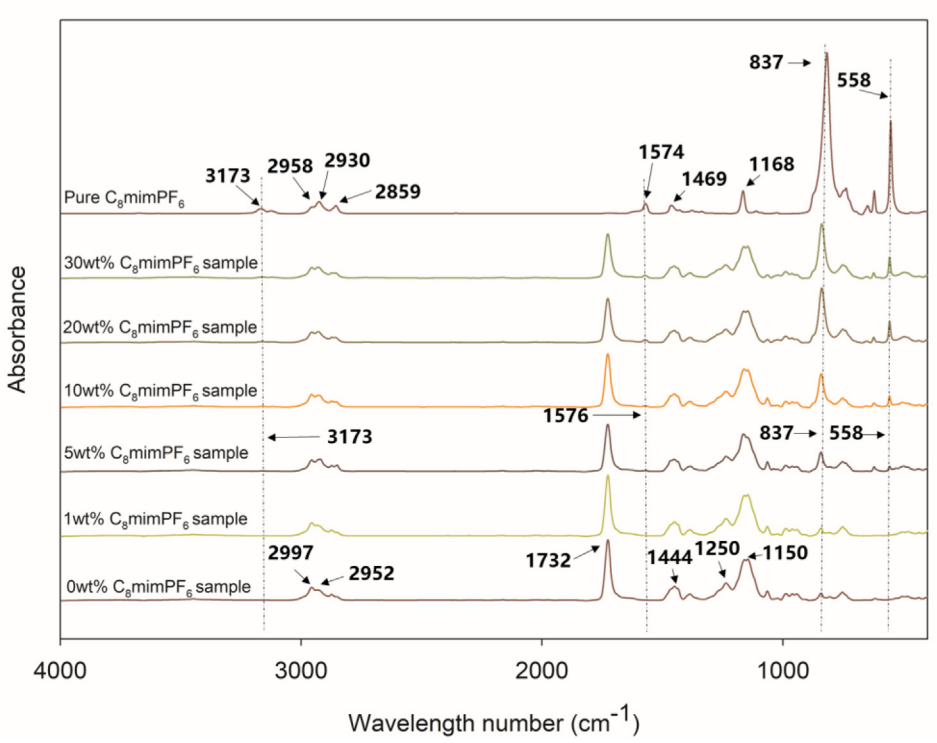

Fig. 7 FTIR spectra for particles containing different C_8mimPF_6 concentrations.

there is no carbon–carbon or carbon–oxygen double bond to break for further polymerization. Hence, the C_8mimPF_6 should not participate in polymerization. Because of the hydrophobicity of the C_8mimPF_6, it should remain in the oil phase rather than dispersed in the water phase. For miniemulsion polymerization, a hydrophobic material encapsulated in polymer may form two structures: the core–shell morphology and homogenous particle [52]. Hu et al. [4] investigated the morphology of PMMA particles containing different amounts of C_8mimPF_6 via TEM and stated that no phase separation was observed. This further indicates that C_8mimPF_6 and PMMA were mixed in a homogenous state. Thus, it can be postulated that C_8mimPF_6 might have permeated into the voids of the PMMA-PBA copolymer (see Fig. 8.).

3.2.2. Adsorption isotherm of C_8mimPF_6

As mentioned above, the protection effect of C_8mimPF_6 was achieved through the adsorption of ILs. For the composites coating in immersion test, the C_8mimPF_6 was encapsulated in PMMA-co-PBA at first. With the prolonging of immersion time, coating surface degraded and C_8mimPF_6 was exposed to the corrosive medium. After that, isolated C_8mimPF_6 was released and adsorbed on the mild steel surface. To understand the possible mechanism of interaction between C_8mimPF_6 and mild steel surface, adsorption isotherm was applied. Here, it is assumed that the adsorption of C_8mimPF_6 obeys Langmuir adsorption isotherm, which was proven to be the optimal adsorption isotherm for corrosion inhibitors [53]. The equation is given as follows.

$$\frac{C_{inh}}{\theta} = \frac{1}{K_{ads}} + C_{inh} \tag{5}$$

where C_{inh} is the inhibitor concentration and θ is the surface coverage fraction. Because the mild steel surface was coated with latex, the concentration of inhibitor can be approximately treated as the concentration of C_8mimPF_6 in the coating. The inhibition efficiency calculated from charge transfer resistance of EIS plot was used to estimate the surface coverage. In a corrosive environment, the inhibition effect of C_8mimPF_6 was achieved by its adsorption on the mild steel surface and blocking of reaction sites. Thus, θ can be represented as the difference in inhibition efficiency between samples with and without C_8mimPF_6. K_{ads} denotes the equilibrium constant of the whole adsorption process. With the plot of $\frac{C_{inh}}{\theta}$ versusC_{inh}, the K_{ads} can be obtained. With K_{ads}, the standard free energy ($\Delta G^0{}_{ads}$) of inhibitor adsorption on mild steel surface can be calculated.

$$\Delta G^0{}_{ads} = -RT(55.5K_{ads}) \tag{6}$$

where 55.5 is the value of the molar concentration of pure water, R and T represent respectively the universal gas constant (8.314 J $(mol{\cdot}K)^{-1}$) and the temperature in Kelvin. $\Delta G^0{}_{ads}$ of C_8mimPF_6 in this experiment was -19.0 kJ mol^{-1}. Empirically, for $\Delta G^0{}_{ads}$ less negative than -20 kJ mol^{-1}, the adsorption is physical adsorption, for $\Delta G^0{}_{ads}$ negative than -40 kJ mol^{-1}, the adsorption is chemical adsorption [22,54]. Therefore, it can be concluded that C_8mimPF_6 in this research adsorbed on mild steel surface through physical adsorption.

3.2.3. Effect of C_8mimPF_6 on hydrophobicity of the coated steel surface

The anticorrosion effect of the added C_8mimPF_6 in the latex coating also benefits from the presence of C_8mimPF_6 enhanc-

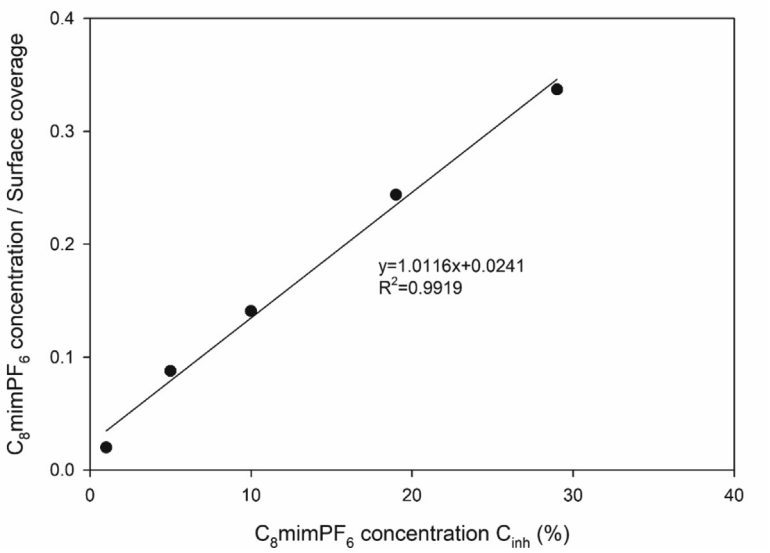

Fig. 8 Langmuir adsorption plots for C_8mimPF_6.

ing the hydrophobicity of the coating due to the hydrophobic nature of PF_6^-. The hydrophobicity of PF_6^- was studied by Qiu et al. [55] who demonstrated that water contact angle of poly (ionic liquid)-grafted silica hybrid materials rose from 84° to 131° when changing the IL anion from Br^- to PF_6^-.

To further validate such hydrophobicity enhancement effect due to the presence of PF_6^-, the contact angle measurement between water droplets and the coating surface in this work is carried out. In Fig. 9, the highest contact angle was found at 82.2° for the 30 wt% C_8mimPF_6 sample and decreased with reducing the C_8mimPF_6 concentration to 58.5° for the C_8mimPF_6 free sample. This trend of contact angle variation is consistent with the literature reported. As a result, the resistance for water penetration into the coating film may be reduced. Hence, the ions transfer would be hindered. This could be proven by further evaluation of ions transfer rate given in next session.

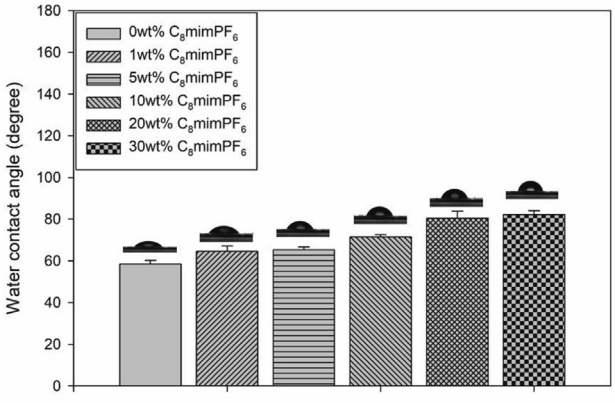

Fig. 9 Variation of contact angle between water and coated mild steel surface as a function of IL (C_8mimPF_6) concentration.

3.2.4. Effect of C_8mimPF_6 on diffusion of corrosive ions through the coating

As mentioned above, the physical adsorption of C_8mimPF_6 and increased hydrophobicity due to the increased concentration of C_8mimPF_6 may hinder the corrosive ions transfer from the bulk solution to the substrate. This is a mass transfer limiting step in which it is mainly diffusion. Based on the simplified Fick's law of diffusion [9,56], the diffusion coefficient D of corrosive ions can be calculated as.

$$\frac{\lg C_c - \lg C_0}{\lg C_\infty - \lg C_0} = \frac{2}{L}\sqrt{\frac{D}{\pi}}\sqrt{t} \tag{7}$$

where C_0, C_c and C_∞ are the coating capacitances at the initial immersion time t_0, current time t_c and the time when the coating reaches the saturated water absorption state t_∞. L is the coating thickness. D is the diffusion coefficient. The results are plotted in Fig. 10. The diffusion coefficient was reduced sharply as the concentration of C_8mimPF_6 increased from 0 wt% to 10 wt%. Such reduction became relatively small as the C_8mimPF_6 concentration further increased from 10 wt% to 30 wt%. Such results are consistent with those found in the EIS test (Table 1) that the anticorrosion effect of C_8mimPF_6 in the PMMA/PBA copolymer latex could be mainly attributed to the barrier effect which hindered the diffusivity of corrosive ions and oxygen in the 3.5 wt% NaCl solution, especially when the C_8mimPF_6 concentration was lower than 20 wt%. However, the barrier effect in the presence of C_8mimPF_6 may be hindered by other factors when the concentration was higher than 10 wt%. Further, that measurement of diffusion cannot truly reflect the overall results as observed in the Tafel plots (Table 3). More work is required.

3.2.5. The role of C_8mimPF_6 in the waterborne PMMA-co-PBA anticorrosion coating

According to the aforementioned discussion, C_8mimPF_6 may exist in the void of PMMA-co-PBA freely without attending chemical reaction. When the coating film without C_8mimPF_6 was immersed in the salty environment, corrosive ions could pass through the pinholes and defects of the coating film and reach the surface of mild steel to induce corrosion [57].

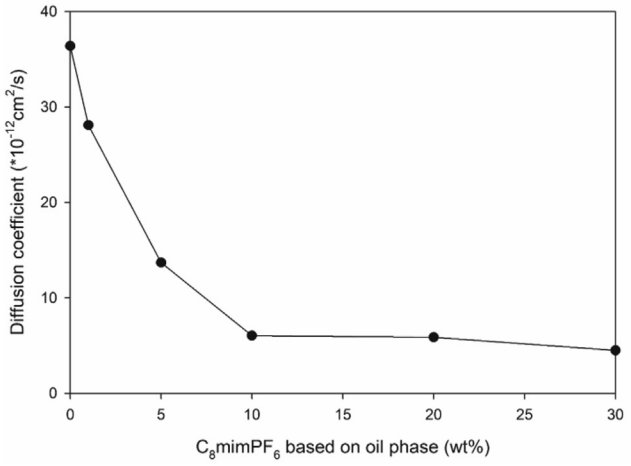

Fig. 10 Variation in diffusion coefficient of the coating layer as a function of C_8mimPF_6 concentration.

If C_8mimPF_6 was introduced, the transfer of corrosive ions would be hindered due to the presence of PF_6^-, which could enhance hydrophobicity of coating as shown in Fig. 9. Moreover, after a long-term exposure to the salty environment, the water adsorption of waterborne acrylic coating film reached saturation and degradation of the coating film started [39]. Further corrosion caused the release of encapsulated C_8mimPF_6. The proposed schematic representation of corrosion inhibition mechanism is shown in Fig. 11. At the initial stage, the adsorption of Cl^- on the mild steel surface dominated the adsorption process due to the abundant NaCl in the solution. The surface became negatively charged and the C_8mim^+ cation replaced Na^+ adsorbed on the surface due to its larger steric hindrance [21–24]. The adsorption of C_8mimPF_6 followed the Langmuir adsorption isotherm. Since it was physical adsorption, no electrons would be transferred between C_8mimPF_6 and other substance. Thus, it can be concluded that C_8mim^+ was adsorbed to the cathodic sites on the surface through electrostatic force. The C_8mim^+ cation blocked the corrosion sites so that it could retard the mass transfer of corrosive ions from the bulk solution to the mild steel surface.

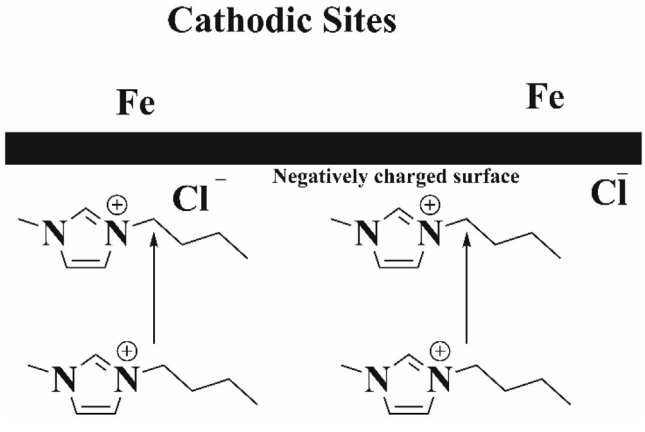

Fig. 11 Corrosion inhibition mechanism of C_8mimPF_6.

This function can be described as a barrier effect. In formula, it can be represented as.

$$Fe + C_8mim^+ \leftrightarrow Fe(C_8mim^+)_{ads}$$

In summary, C_8mimPF_6 played a dual role in the anticorrosion process, where PF_6^- improved hydrophobicity of the coating and C_8mim^+ played a barrier effect in the coating film in the salty environment via physical adsorption.

4. Conclusion

A new waterborne acrylic formulation containing the ionic liquid C_8mimPF_6 was developed for anticorrosion. The electrochemical technique OCP, EIS, Tafel results confirmed that increasing the C_8mimPF_6 concentration from 0 to 30 wt% could significantly improve the anticorrosion inhibition efficiency, i.e., from 41 % to 89 % based on the charge transfer resistance, and from 64% to 87% based on the corrosion current density. A comparison between the SEM images of PMMA-co-PBA composite coatings with different concentrations of C_8mimPF_6 also revealed that the introduction of C_8mimPF_6 into the coating could reduce the defects in the final coating. The role of C_8mimPF_6 in the anticorrosion effect was further studied and the FTIR spectra of latex samples were analyzed. No new species emerged after miniemuslion polymerization, which suggested that no chemical reaction occurred between C_8mimPF_6 and the polymer matrix.

The anticorrosion effect was mainly ascribed to the physical adsorption of cation of C_8mimPF_6 that blocked the reaction sites on the surface of mild steel. When the PMMA-co-PBA coating film was damaged and C_8mimPF_6 was released, the adsorption of the cation of C_8mimPF_6 followed the Langmuir adsorption isotherm. Another explanation is that the increased hydrophobicity resulted from the hydrophobic anion of C_8mimPF_6. This was confirmed by the result from measurement of the contact angle between water and coated samples for the latex with various concentrations of C_8mimPF_6. The contact angle did increase from 58.5° to 82.2° as the concentration of C_8mimPF_6 increased from 0 wt% to 30 wt%. Thus, the anticorrosion effect in the presence of C_8mimPF_6 could be attributed to the reduction of wettability of water to the coating surface. Such an effect may be a trade-off by lowering the PMMA-co-PBA content in the latex coating with excessive C_8mimPF_6. Our calculated diffusivity data obtained via simplified Fick's law of diffusion indicates the reduction of diffusion coefficient from 3.6×10^{-11} cm^2 s^{-1} to 4.5×10^{-12} cm^2 s^{-1} with increasing the concentration of C_8mimPF_6 from 0 wt% to 30 wt%, which manifests the enhancement of the barrier effect.

Although the improvement of anticorrosion performance of the C_8mimPF_6 containing latex coatings may be not satisfactory compared to other typical oil type anticorrosion coatings, this study enlightens a way to the development of more useful functional groups for corrosion inhibition, which can be either applied in an ionic liquid or encapsulated in a waterborne acrylic coating.

5. Future prospective

This research has proven the anticorrosion effect of C_8mimPF_6 encapsulated in PMMA-co-PBA. However, the anticorrosion

improvement is far from being optimal, where the highest inhibition efficiency is 89%. To further improve the inhibition performance of coating, further fine tuning the formulation including the using different type of ionic liquid. For C_8-mimPF_6, cation is the main effective part in corrosion inhibition. As for the anion, PF_6^- promoted its hydrophobicity but does not play a role in adsorption. Therefore, if the anions attend the inhibition, cations and anions can achieve synthetic effect so that anticorrosion performance can be further enhanced.

Declaration of Competing Interest

The authors declare that they have no known competing financial interests or personal relationships that could have appeared to influence the work reported in this paper.

Acknowledgements

The research is financially supported by Ningbo Yuxi Material Protection Ltd (Grant numbers: 01.03.07.01.2015.06.002) and PhD scholarship from University of Nottingham Ningbo China.

References

[1] Y. Kong, B. Hu, K.-L. Choy, X. Li, G. Chen, Study of miniemulsion formulation containing 1-octyl-3-methylimidazolium hexafluorophosphate for its application in low-emitting coating products, Soft Matter 11 (7) (2015) 1293–1302.
[2] Y. Kong, "Encapsulation of room temperature ionic liquids by miniemulsion polymerisation for application in low-emitting latex coating," ed, 2016.
[3] Y. Kong, B. Hu, Y. Guo, Y. Wu, Effect of ionic liquids on stability of O/W miniemulsion for application of low emission coating products, Chin. J. Chem. Eng. 24 (1) (2016) 196–201.
[4] B. Hu, Y. Kong, R. Zheng, J. Dong, K.-L. Choy, H. Zhao, Effect of C 8 mimPF 6 on miniemulsion polymerization for application in new latex coating products, Faraday Discuss. 190 (2016) 487–508.
[5] M. Cui, S. Ren, J. Pu, Y. Wang, H. Zhao, L. Wang, Poly (o-phenylenediamine) modified graphene toward the reinforcement in corrosion protection of epoxy coatings, Corros. Sci. 159 (2019) 108131.
[6] Y. He, Y. Boluk, J. Pan, A. Ahniyaz, T. Deltin, P.M. Claesson, Corrosion protective properties of cellulose nanocrystals reinforced waterborne acrylate-based composite coating, Corros. Sci. 155 (2019) 186–194.
[7] E. Carretti, L. Dei, Physicochemical characterization of acrylic polymeric resins coating porous materials of artistic interest, Prog. Org. Coat. 49 (3) (2004) 282–289.
[8] B. Du, F. Chen, R. Luo, S. Zhou, Z. Wu, Synthesis and characterization of nano-TiO2/SiO2-acrylic composite resin, Adv. Mater. Sci. Eng. 2019 (2019) 1–7.
[9] J. Ding, S. Shi, H. Yu, Study on modification of lignin as dispersant of aqueous graphene suspension and corrosion performance in waterborne G/epoxy coating, IJAERS 3 (9) (2016) 101–112.
[10] M. Kendig, R. Buchheit, Corrosion inhibition of aluminum and aluminum alloys by soluble chromates, chromate coatings, and chromate-free coatings, Corrosion 59 (5) (2003) 379–400.
[11] D. Winkler, M. Breedon, P. White, A. Hughes, E. Sapper, I. Cole, Using high throughput experimental data and in silico models to discover alternatives to toxic chromate corrosion inhibitors, Corros. Sci. 106 (2016) 229–235.
[12] C. Verma, E.E. Ebenso, M. Quraishi, Ionic liquids as green and sustainable corrosion inhibitors for metals and alloys: An overview, J. Mol. Liq. 233 (2017) 403–414.
[13] M.J. Earle, K.R. Seddon, Ionic liquids. Green solvents for the future, Pure Appl. Chem. 72 (7) (2000) 1391–1398.
[14] M. Kar, K. Matuszek, and D. R. MacFarlane, "Ionic Liquids," in Kirk-Othmer Encyclopedia of Chemical Technology: John Wiley & Sons, 2019.
[15] H. Ashassi-Sorkhabi, M. Es'haghi, Corrosion inhibition of mild steel in acidic media by [BMIm] Br Ionic liquid, Mater. Chem. Phys. 114 (1) (2009) 267–271.
[16] O.A. Al-Rashed, A.A. Nazeer, Ionic liquids with superior protection for mild steel in acidic media: effects of anion, cation, and alkyl chain length, J. Mol. Liq. 288 (2019) 111015.
[17] Y. Sasikumar, A.S. Adekunle, L.O. Olasunkanmi, I. Bahadur, R. Baskar, M.M. Kabanda, I.B. Obot, E.E. Ebenso, Experimental, quantum chemical and Monte Carlo simulation studies on the corrosion inhibition of some alkyl imidazolium ionic liquids containing tetrafluoroborate anion on mild steel in acidic medium, J. Mol. Liq. 211 (2015) 105–118.
[18] C. Verma, D.K. Verma, E.E. Ebenso, M.A. Quraishi, "Sulfur and phosphorus heteroatom-containing compounds as corrosion inhibitors: An overview, Heteroatom Chem. 29(4) (2018) e21437.
[19] M. Vinutha, T. Venkatesha, Review on mechanistic action of inhibitors on steel corrosion in acidic media, Portugaliae Electrochim. Acta 34 (3) (2016) 157–184.
[20] S.-H. Yoo, Y.-W. Kim, K. Chung, N.-K. Kim, J.-S. Kim, Corrosion inhibition properties of triazine derivatives containing carboxylic acid and amine groups in 1.0 M HCl solution, Ind. Eng. Chem. Res. 52 (32) (2013) 10880–10889.
[21] N.V. Likhanova, M.A. Domínguez-Aguilar, O. Olivares-Xometl, N. Nava-Entzana, E. Arce, H. Dorantes, The effect of ionic liquids with imidazolium and pyridinium cations on the corrosion inhibition of mild steel in acidic environment, Corros. Sci. 52 (6) (2010) 2088–2097.
[22] X. Li, S. Deng, H. Fu, G. Mu, Synergistic inhibition effect of rare earth cerium (IV) ion and anionic surfactant on the corrosion of cold rolled steel in H2SO4 solution, Corros. Sci. 50 (9) (2008) 2635–2645.
[23] F. Bentiss, M. Lebrini, M. Lagrenée, Thermodynamic characterization of metal dissolution and inhibitor adsorption processes in mild steel/2, 5-bis (n-thienyl)-1, 3, 4-thiadiazoles/hydrochloric acid system, Corros. Sci. 47 (12) (2005) 2915–2931.
[24] S. Velusamy, S. Sakthivel, L. Neelakantan, J.S. Sangwai, Imidazolium-based ionic liquids as an anticorrosive agent for completion fluid design, J. Earth Sci. 28 (5) (2017) 949–961.
[25] Z. Cao, Y. Xia, C. Chen, Fabrication of novel ionic liquids-doped polyaniline as lubricant additive for anti-corrosion and tribological properties, Tribol. Int. 120 (2018) 446–454.
[26] M.G. Freire, L.M. Santos, A.M. Fernandes, J.A. Coutinho, I. M. Marrucho, An overview of the mutual solubilities of water–imidazolium-based ionic liquids systems, Fluid Phase Equilib. 261 (1–2) (2007) 449–454.
[27] V. Mittal, "Miniemulsion polymerization technology," vol. 34: John Wiley & Sons, 2011, ch. 1, pp. 3-10.
[28] A.A.H. Kadhum, A.B. Mohamad, H.D. Jaffar, S.S. Yan, J. Hilo, Corrosion of Nickel-Aluminum-Bronze alloy in aerated 0.1 M sodium chloride solutions under hydrodynamic condition, Int. J. Electrochem. Sci 8 (2013) 4571–4582.
[29] M.E. Orazem, B. Tribollet, Electrochemical impedance spectroscopy, John Wiley & Sons, 2011.
[30] M.E. Orazem, N. Pébère, B. Tribollet, Enhanced graphical representation of electrochemical impedance data, J. Electrochem. Soc. 153 (4) (2006) B129.

[31] E. McCafferty (Ed.), Introduction to Corrosion Science, Springer New York, New York, NY, 2010.
[32] G. Baril, C. Blanc, N. Pébère, AC impedance spectroscopy in characterizing time-dependent corrosion of AZ91 and AM50 magnesium alloys characterization with respect to their microstructures, J. Electrochem. Soc. 148 (12) (2001) B489.
[33] C. Liu, S. Qiu, P. Du, H. Zhao, L. Wang, An ionic liquid–graphene oxide hybrid nanomaterial: synthesis and anticorrosive applications, Nanoscale 10 (17) (2018) 8115–8124.
[34] O. Lewis, G. Critchlow, G. Wilcox, A. deZeeuw, J. Sander, A study of the corrosion resistance of a waterborne acrylic coating modified with nano-sized titanium dioxide, Prog. Org. Coat. 73 (1) (2012) 88–94.
[35] C. Jiao et al, Advances in waterborne acrylic resins: synthesis principle, modification strategies, and their applications, ACS Omega 6 (4) (2021) 2443–2449.
[36] K. Farhadi, H. Zebhi, P.N. Moghadam, M. Es'haghi, H. Ashassi-Sorkhabi, Electrochemical preparation of nano-colloidal polyaniline in polyacid matrix and its application to the corrosion protection of 430SS, Synth. Met. 195 (2014) 29–35.
[37] O. Dagdag et al, Fabrication of polymer based epoxy resin as effective anti-corrosive coating for steel: Computational modeling reinforced experimental studies, Surf. Interfaces 18 (2020) 100454.
[38] A. Mostafaei, F. Nasirpouri, Epoxy/polyaniline–ZnO nanorods hybrid nanocomposite coatings: Synthesis, characterization and corrosion protection performance of conducting paints, Prog. Org. Coat. 77 (1) (2014) 146–159.
[39] A. Miszczyk, K. Darowicki, Water uptake in protective organic coatings and its reflection in measured coating impedance, Prog. Org. Coat. 124 (2018) 296–302.
[40] C. Malmberg, A. Maryott, Dielectric constant of water from 00 to 1000 C, J. Res. Nat. Bur. Stand. 56 (1) (1956) 1.
[41] S. Pour-Ali, C. Dehghanian, A. Kosari, In situ synthesis of polyaniline–camphorsulfonate particles in an epoxy matrix for corrosion protection of mild steel in NaCl solution, Corros. Sci. 85 (2014) 204–214.
[42] D. Brasher, A. Kingsbury, Electrical measurements in the study of immersed paint coatings on metal. I. Comparison between capacitance and gravimetric methods of estimating water-uptake, J. Appl. Chem. 4 (2) (1954) 62–72.
[43] C.J. Weng, J.Y. Huang, K.Y. Huang, Y.S. Jhuo, M.H. Tsai, J. M. Yeh, Advanced anticorrosive coatings prepared from electroactive polyimide–TiO hybrid nanocomposite materials, Electrochim. Acta 55 (28) (2010) 8430–8438.
[44] J.M. Yeh, H.Y. Huang, C.L. Chen, W.F. Su, Y.H. Yu, Siloxane-modified epoxy resin–clay nanocomposite coatings with advanced anticorrosive properties prepared by a solution dispersion approach, Surf. Coat. Technol. 200 (8) (2006) 2753–2763.
[45] M.P. Scott, M. Rahman, C.S. Brazel, Application of ionic liquids as low-volatility plasticizers for PMMA, Eur. Polym. J. 39 (10) (2003) 1947–1953.
[46] T. Iimori et al, Local structure at the air/liquid interface of room-temperature ionic liquids probed by infrared– visible sum frequency generation vibrational spectroscopy: 1-alkyl-3-methylimidazolium tetrafluoroborates, J. Phys. Chem. B 111 (18) (2007) 4860–4866.
[47] R. Aroca, M. Nazri, G. Nazri, A. Camargo, M. Trsic, Vibrational spectra and ion-pair properties of lithium hexafluorophosphate in ethylene carbonate based mixed-solvent systems for lithium batteries, J. Solution Chem. 29 (10) (2000) 1047–1060.
[48] B. Peng, J. Zhang, R. Lu, S. Zhang, W. Zhou, H. Gao, Dispersive micro-solid phase extraction based on self-assembling, ionic liquid-coated magnetic particles for the determination of clofentezine and chlorfenapyr in environmental water samples, Analyst 138 (22) (2013) 6834–6843.
[49] G. Duan, C. Zhang, A. Li, X. Yang, L. Lu, X. Wang, Preparation and characterization of mesoporous zirconia made by using a poly (methyl methacrylate) template, Nanoscale Res. Lett. 3 (3) (2008) 118.
[50] S. Ramesh, K.H. Leen, K. Kumutha, A. Arof, FTIR studies of PVC/PMMA blend based polymer electrolytes, Spectrochim. Acta Part A Mol. Biomol. Spectrosc. 66 (4–5) (2007) 1237–1242.
[51] G. Odian, Principles of polymerization ch. 3 (2004) 198–204.
[52] P.B. Cardoso, P.H. Araújo, C. Sayer, Encapsulation of jojoba and andiroba oils by miniemulsion polymerization. Effect on molar mass distribution, in *Macromolecular Symposia*, 2013, vol. 324, no. 1: Wiley Online Library, pp. 114-123.
[53] S. Cao, D. Liu, H. Ding, J. Wang, H. Lu, J. Gui, Corrosion inhibition effects of a novel ionic liquid with and without potassium iodide for carbon steel in 0.5 M HCl solution: An experimental study and theoretical calculation, J. Mol. Liq. 275 (2019) 729–740.
[54] F.M. Donahue, K. Nobe, Theory of organic corrosion inhibitors: adsorption and linear free energy relationships, J. Electrochem. Soc. 112 (9) (1965) 886.
[55] H. Qiu, T. Sawada, S. Jiang, H. Ihara, Synthesis and characterization of poly (ionic liquid)-grafted silica hybrid materials through surface radical chain-transfer polymerization and aqueous anion-exchange, Mater. Lett. 64 (14) (2010) 1653–1655.
[56] C. Perez, A. Collazo, M. Izquierdo, P. Merino, X. Novoa, Characterisation of the barrier properties of different paint systems: Part I. Experimental set-up and ideal Fickian diffusion, Prog. Org. Coat. 36 (1–2) (1999) 102–108.
[57] R.M. Souto, Y. González-García, J. Izquierdo, S. González, Examination of organic coatings on metallic substrates by scanning electrochemical microscopy in feedback mode: revealing the early stages of coating breakdown in corrosive environments, Corros. Sci. 52 (3) (2010) 748–753.